

1 **Evaluation of inverse estimates of North American net**
2 **ecosystem exchange of CO₂ from different observing**
3 **systems using ACT-America airborne observations**

4 **Yu Yan Cui¹, Andrew R. Jacobson^{2,3}, Sha Feng¹, Daniel Wesloh¹, Tobias**
5 **Gerken^{1,4}, Zachary R. Barkley¹, Klaus Keller^{5,7}, David Baker⁶, and Kenneth J**
6 **Davis^{1,7}**

7 ¹Department of Meteorology and Atmospheric Science, The Pennsylvania State University, University
8 Park, PA, USA

9 ²Cooperative Institute for Research in Environmental Sciences, University of Colorado, Boulder, CO, USA

10 ³NOAA Earth System Research Laboratory, Global Monitoring Laboratory, Boulder, CO, USA

11 ⁴now at School of Integrated Sciences, James Madison University, Harrisonburg, VA, USA

12 ⁵Department of Geosciences, The Pennsylvania State University, University Park, PA, USA

13 ⁶Cooperative Institute for Research in the Atmosphere, Colorado State University, Fort Collins, CO, USA

14 ⁷Earth and Environmental Systems Institute, The Pennsylvania State University, University Park, PA,

15 USA

16 **Key Points:**

- 17 • The IS and LNLG inversions are the most reliable products of CarbonTracker in
18 temperate North America, superior to OG or LNLGOGIS inversions.
- 19 • Errors in these CarbonTracker regional flux estimates are not strongly dependent
20 on the observational data sources.
- 21 • CarbonTracker overestimates seasonal NEE for the Eastern and Central US, as
22 a result, the annual NEE from CarbonTracker may underestimate continental up-
23 take of CO₂.

Corresponding author: Yu Yan Cui, yqc5573@psu.edu

Abstract

Quantification of regional terrestrial carbon dioxide (CO_2) fluxes is critical to our understanding of the carbon cycle. We evaluate inverse estimates of net ecosystem exchange (NEE) of CO_2 fluxes in temperate North America, and their sensitivity to the observational data used to drive the inversions. Specifically, we consider the state-of-the-science CarbonTracker global inversion system, which assimilates (i) in situ measurements (“IS”), (ii) the Orbiting Carbon Observatory-2 (OCO-2) v9 column CO_2 (XCO_2) retrievals over land (“LNLG”), (iii) OCO-2 v9 XCO_2 retrievals over ocean (“OG”), and (iv) a combination of all these observational constraints (“LNLGOGIS”). We use independent CO_2 observations from the Atmospheric Carbon and Transport (ACT) - America aircraft mission to evaluate the inversions. We diagnose errors in the flux estimates using the differences between modeled and observed biogenic CO_2 mole fractions, influence functions from a Lagrangian transport model, and root-mean-square error (RMSE) and bias metrics. The IS fluxes have the smallest RMSE among the four products, followed by LNLG. Both IS and LNLG outperform the OG and LNLGOGIS inversions with regard to RMSE. Regional errors do not differ markedly across the four sets of posterior fluxes. The CarbonTracker inversions appear to overestimate the seasonal cycle of NEE in the Midwest and Western Canada, and overestimate dormant season NEE across the Central and Eastern US. The CarbonTracker inversions may overestimate annual NEE in the Central and Eastern US. The success of the LNLG inversion with respect to independent observations bodes well for satellite-based inversions in regions with more limited in situ observing networks.

Plain Language Summary

Biological CO_2 fluxes, an important component of the earth’s climate system, remain uncertain, especially at continental and sub-continental spatial domains. Different global CO_2 observing systems imply significantly different net biological fluxes of CO_2 . We use independent CO_2 measurements from an extensive multi-seasonal aircraft campaign to evaluate biological CO_2 flux estimates derived from four different observational systems entered into a common data analysis system. The observations include both ground- and satellite-based measurements. We found that one of the the satellite-based CO_2 estimates performs nearly as well as the estimates based on ground-based measurements. This suggests that the satellite data may serve to estimate regional variations in biological CO_2 fluxes in portions of the globe with more limited ground-based observing networks. The inversions appear to overestimate dormant season release of biological CO_2 to the atmosphere, thus may underestimate the net uptake of CO_2 by ecosystems in the Central and Eastern United States.

1 Introduction

Accurate quantification of carbon dioxide (CO_2) fluxes from different sources is an important input to the design of climate policies (e.g. Masson-Delmotte et al., 2018; Keller et al., 2008; Ciais et al., 2014). CO_2 flux related to terrestrial net ecosystem exchange (NEE) is one of the major components. It is challenging to quantify CO_2 NEE fluxes due to complex biosphere processes, together with the biosphere- atmosphere interactions (e.g. Tian et al., 2016). Both bottom-up and top-down approaches (e.g. Pan et al., 2011; Hayes et al., 2012; Liu et al., 2017; Hu et al., 2019; Thompson et al., 2020) have been used to characterize and quantify CO_2 NEE fluxes using data from a wide range of observation platforms.

The top-down approach is an optimization framework to improve a priori flux estimates, that are informed, for example, by ecosystem carbon-stock inventories or carbon flux models (e.g. Haynes et al., 2019). Atmospheric CO_2 measurements, on which the top-down method relies, can contribute powerful constraints to the bottom-up meth-

74 ods (e.g. Ogle et al., 2015). Different atmospheric CO₂ measurement platforms such as
75 boundary-layer CO₂ mole fractions from ground-based networks (e.g. Andrews et al.,
76 2014; Miles et al., 2012) and column-averaged CO₂ mole fractions (XCO₂) from satel-
77 lites (e.g. Liu et al., 2020), aim to complement each other. Measurement biases, atmo-
78 spheric transport errors, or representation errors, however, may cause difficulty in as-
79 simulating these measurements within the optimization process.

80 Evaluating current top-down CO₂ flux estimates from the different platforms with
81 independent observations is a promising avenue to improve them. Chevallier et al. (2019)
82 compares six global CO₂ atmospheric inversions from the combinations of three mea-
83 surements platforms (i.e Orbiting Carbon Observatory-2 - OCO-2 or Greenhouse Gas
84 Observing Satellite - GOSAT column retrievals, and boundary-layer in situ measurements)
85 using a large number of aircraft measurements in the free troposphere. They provide a
86 cross-comparison among different inversion estimates as well as mole fraction-based com-
87 parisons between inversions and the aircraft measurements. They found that differences
88 in annual budgets are mainly located in the northern and tropical portions of the globe.
89 The OCO-2-based inversion produced results close to the traditional in situ inversion,
90 but the data they used did not allow them to distinguish between the quality of OCO-
91 2-based fluxes and in situ-based fluxes. The global inversions are temporally and spa-
92 tially resolved products, and many aircraft field campaigns take place at a regional scale.
93 This opens up the opportunity for further in-depth regional evaluations.

94 The Atmospheric Carbon and Transport – America (ACT-America) mission, con-
95 ducted flights east of the Rocky Mountains in the United States (US) during Summer
96 2016, Winter 2017, Fall 2017, Spring 2018, and Summer 2019 (Davis et al., 2018). The
97 multi-seasonal aircraft CO₂ sampling of ACT-America provides a unique opportunity
98 for regional evaluation of CO₂ flux estimates. Extensive atmospheric CO₂ measurements
99 from the atmospheric boundary layer to the upper free troposphere during four seasons
100 from ACT-America enable researchers to rigorously assess and potentially distinguish
101 the biases and accuracy of different inversion estimates for temperate North America.

102 OCO-2 gathers XCO₂ measurements globally using nadir and glint observations
103 over land, and glint observations over the oceans (Eldering, O’Dell, et al., 2017; Elder-
104 ington, Wennberg, et al., 2017). The OCO-2 retrievals are continually being improved (e.g.
105 Crowell et al., 2019; Miller & Michalak, 2020). Independent observation campaigns can
106 test the ability of the OCO-2 v9-based inversions to estimate regional-scale fluxes with
107 accuracy and precision. Temperate North America has one of the densest in situ-based
108 greenhouse gas monitoring networks in the world. An evaluation of the OCO-2 v9 based
109 flux estimates, along with the evaluation of in situ-based CO₂ flux estimates together
110 can be used to assess the complementary role of the two platforms. Additionally, a multi-
111 platform strategy that combines in situ- and satellite- based platforms to constrain CO₂
112 NEE is promising but requires independent evaluation.

113 In this study, we implement a method to evaluate the in situ-based, OCO-2 v9-based,
114 and two-system-combined inversions of CO₂ NEE in temperate North America using air-
115 borne observations from the ACT-America mission. Specifically, We evaluate the state-
116 of-the-science CarbonTracker global inversion system’s inverse NEE estimate for North
117 America from four different set of observations, created as part of OCO-2 v9 model in-
118 tercomparison project (MIP) (https://www.esrl.noaa.gov/gmd/ccgg/OC02_v9mip/).
119 We evaluate the capability of the four different observing systems to quantify CO₂ NEE
120 in temperate North America. The details of the evaluation framework are described in
121 Section 2. Results and discussion are presented in Section 3. We conclude in Section 4.

Table 1. Aircraft data from four ACT-America campaigns used in the study

	Flight months	Flight days	Flight (hours)	ABL data (%)
Summer 2016	Jul-Aug	25	248	34
Winter 2017	Feb-Mar	25	218	35
Fall 2017	Oct-Nov	22	245	33
Spring 2018	Apr-May	26	261	32

122 2 Materials and Methods

123 2.1 CarbonTracker CO₂ NEE flux products

124 We evaluate four CO₂ flux products in the study, which are from CarbonTracker
 125 global inversion system (Jacobson et al., 2020). Following the protocol of OCO-2 v9 MIP,
 126 CarbonTracker performed a series of global CO₂ flux experiments for 2015-2019 driven
 127 by a variety of observation platforms, including CO₂ measurements from 1) in situ data
 128 (IS) compiled in the GLOBALVIEW+ 5.0 (Cooperative Global Atmospheric Data In-
 129 tegration Project, 2019) and NRT v5.1 (CarbonTracker Team, 2019) ObsPack products;
 130 2) the land nadir/land glint (LNLG) retrievals of column-integrated CO₂ from OCO-2
 131 v9; 3) OCO-2 ocean glint (OG) v9 retrievals; and 4) a combination of the in-situ and satel-
 132 lite data (LNLGOGIS). These global flux products are mapped onto 1-degree grid cells
 133 at 3-hourly intervals (Figure S1).

134 2.2 ACT-America aircraft campaign

135 We use CO₂ measurements from the Summer 2016, Winter 2017, Fall 2017, and
 136 Spring 2018 ACT-America campaigns. These are the times for which CO₂ flux products
 137 are available from CarbonTracker, as part of the OCO-2 v9 MIP. Each ACT-America
 138 campaign flew over the same three sub-regions of the United States (US): the Mid-Atlantic,
 139 Midwest, and Gulf Coast. For most flight days, two aircraft (a NASA Langley B200 and
 140 a NASA Wallops C130) flew together measuring atmospheric CO₂ mole fractions and
 141 other atmospheric variables in patterns designed to sample the variability in atmospheric
 142 GHGs within mid-latitude weather systems and the associated regional surface fluxes.
 143 All flights were conducted during midday hours (15-0 UCT) in order to sample well mixed
 144 atmospheric boundary layer (ABL) conditions. The detailed instrument, deployment and
 145 dataset of ACT-America are described in (Davis et al., 2018; Wei et al., in prep for this
 146 issue). The calibration of the CO₂ measurements are described by (Baier et al., 2020).
 147 About 35% of the flight time was within the ABL, the portion of the atmosphere most
 148 sensitive to regional GHG surface fluxes. In this study, we use the ABL measurements
 149 excluding the take-off and landing portions, and aggregate these CO₂ measurements across
 150 30-s intervals (Figure 1, Table 1) to construct the receptors in the Lagrangian particle
 151 dispersion modeling that described in section 2.3.

152 2.3 Influence functions for ACT flight data

153 Upwind fluxes influence the aircraft samples. We explicitly quantify the source-receptor
 154 relationship (i.e influence function) using a Lagrangian particle dispersion model (FLEXPART-
 155 WRF) (Brioude et al., 2013) in a backward mode. The simulations of FLEXPART-WRF
 156 are driven by the 27-km WRF-Chem simulated meteorology from the base line simula-
 157 tion described in Feng et al. (2019a, 2019b) which were nudged to the 25-km ECMWF-
 158 ERA5 reanalysis data (Hersbach et al., 2020).

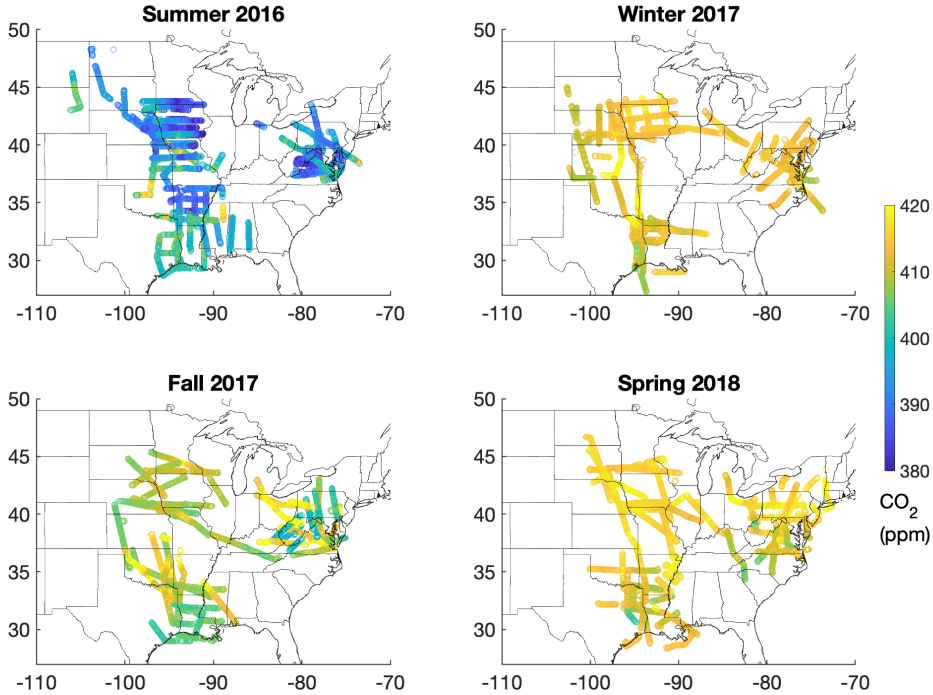


Figure 1. Boundary layer CO₂ mole fractions (unit: ppmv) sampled during four ACT-America campaigns.

159 We computed a suite of influence functions across 98 flight days, at the same spa-
 160 tial and temporal resolution of the meteorological driver (27 km and hourly) covering
 161 the entire domain (Figure 2). Each receptor of the influence function is the 30-s inter-
 162 val along flight tracks, characterized by a box with boundaries between the maximum
 163 and minimum latitude/longitude as well as between the maximum and minimum heights
 164 during the 30-s interval. Each receptor box released 5,000 particles and simulated their
 165 transport and dispersion backward for 10 days (Cui et al., 2015, 2017, 2019). A valida-
 166 tion of the suite of influence functions was conducted. Based on the same flux inputs,
 167 background values, and meteorological fields, we compared the FLEXPART-WRF simu-
 168 lated CO₂ mole fractions with the WRF-Chem forward simulations along flight tracks
 169 and found that they agreed well. The suite of influence functions plays a key role in our
 170 evaluation described in Section 2.4.2.

171 **2.4 Biogenic CO₂ component**

172 **2.4.1 Background determination**

173 To evaluate the surface fluxes in our domain, we subtract the CO₂ background val-
 174 ues from the ACT CO₂ measurements to obtain an estimate of the CO₂ mole fraction
 175 enhancements and depletions caused by surface fluxes in the domain. A tracer indicat-
 176 ing CO₂ mole fractions from the boundary condition of the domain (characterized with
 177 the CarbonTracker CO₂ 4-D simulations) is explicitly simulated in the WRF-Chem con-
 178 figuration (Feng et al., 2019a). We interpolated tracer values at each receptor point to
 179 represent the background-value elements in y_{bkg} . For the ACT Summer 2016 campaign,
 180 we used the 4-D simulations of atmospheric CO₂ mole fractions from the CarbonTracker

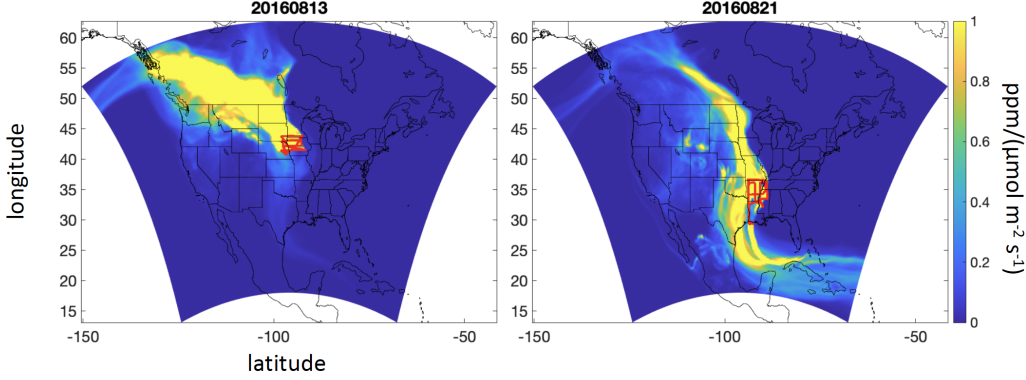


Figure 2. Examples of influence functions (unit: ppm/($\mu\text{mol m}^{-2} \text{s}^{-1}$)) used to quantify the relationship between the upwind sources and downwind receptors along the flights. Ten-day cumulative influence functions for two flight days are shown, including a fair-weather day, 13 August 2016 (left) and a frontal day, 21 August 2016 (right).

181 2017 product, while for the rest of the campaigns we used values from the CarbonTracker
 182 2019-Near Real Time version 2 product. Upper free tropospheric mole fractions can pro-
 183 vide another estimate of continental background conditions (Baier et al., 2020). We com-
 184 pare the simulated background mole fractions along ACT-America flight tracks above
 185 4,000 MSL with the corresponding ACT-America measurements and find good agree-
 186 ment (Figure S2). We do not explicitly compute uncertainty in the background in this
 187 study, but this comparison, and the work of Feng et al. (2019a) suggests that the un-
 188 certainty is less than about 1 ppm.

189 **2.4.2 ACT referenced biogenic CO₂**

190 The atmospheric CO₂ mole fraction continental enhancements and depletions in-
 191 clude the influence of different fluxes: biogenic, fossil fuel, fire, and oceanic. To focus on
 192 the land biogenic CO₂ component, we remove the influence of the fossil fuel, fire, and
 193 oceanic sources on total CO₂(y) by subtracting the component mole fraction enhance-
 194 ments simulated using the influence functions and flux estimates:

195
$$y_{ACTbio} = y - y_{bkg} - HE_{ff} - HE_{fire} - HE_{ocn} \quad (1)$$

196 , where H represents the influence functions (see details in 2.3), which are used with the
 197 fluxes to produce the atmospheric CO₂ mole fractions along flight tracks. E_{ff} , E_{fire} ,
 198 E_{ocn} represent CO₂ fluxes from the fossil fuel, fire, and oceanic sources in the domain.
 199 E_{ff} , E_{fire} , E_{ocn} are obtained from the CarbonTracker system as part of OCO2 v9 MIP.
 200 E_{ff} is obtained from the ODIAC2018 fossil fuel emission inventory, E_{fire} is from the
 201 GFED4.1s wildfire inventory respectively, and E_{ocn} is from the posterior ocean fluxes
 202 of the IS, LNLG, OG, or LNLGOGIS experiments, respectively.

203 Meanwhile, the modeled biogenic CO₂ enhancements/depletions along the ACT
 204 flight tracks are also calculated as well from the four CO₂ NEE flux products (E_{bio} , see
 205 section 2.1) respectively:

206
$$y_{modelbio} = HE_{bio} \quad (2)$$

207

2.5 Evaluation framework and experimental design

208

209

210

211

212

213

To distinguish and rank the different flux products, we calculate the root-mean-square error (RMSE) between $y_{modelbio}$ and y_{ACTbio} . The value of $y_{modelbio}$ is calculated using the influence functions and the flux products at the native spatial and temporal resolutions (i.e 3-hourly, 1x1 degree). The flux product associated with the smaller RMSE value indicates the better performance, and vice versa. The RMSE analysis is applied for all data during each campaign as well as the entire four campaign datasets.

214

215

216

217

218

219

220

221

The mole fraction-based analysis above is the net result of upwind biogenic fluxes. It is hence difficult to identify the sub-regional and ecosystem-specific sources of these divergences between the aircraft observations and simulations from the flux products without further diagnosis (Rayner, 2020). Therefore, in the study, we also conduct the flux-based evaluation to further diagnose the errors of flux products at the sub-regional scale. We apply the Bayesian solution to optimize the flux products using the ACT-America data and define an equation to be the differences between the flux products and their optimizations by ACT-America.

222

$$\varepsilon = BH^T(HBH^T + R)^{-1}(y_{modelbio} - y_{ACTbio}) \quad (3)$$

223

224

225

226

227

228

229

230

231

, where H (dimension: $m \times n$, m : receptors, n : states (spatial clusters associated with the time intervals)) is the influence function, R (dimension: $m \times m$) and B (dimension: $n \times n$) represent the covariance of the model-data mismatch and the prior flux errors, respectively. ε (dimension: $n \times 1$) is a spatially- and temporally- resolved quantity and it represents the errors in the flux product compared with the ACT-America referenced fluxes. ε is in units of $\mu\text{mol}/\text{m}^2/\text{s}$ and it has positive and negative signs. A lower magnitude of ε indicates the flux product is closer to the ACT referenced value. Positive values in ε identify grid clusters where flux products overestimate the NEE of CO_2 , and vice versa.

232

233

234

235

236

237

238

239

240

241

242

243

244

245

246

247

248

249

We explicitly solve ε in the function (equation 3). R is assumed to be squared residual between $y_{modelbio}$ and y_{ACTbio} . B is given to be 100% relative uncertainty of the flux product initially, and we then apply a regularization parameter to B to tune the balance between the contributions of the model-data mismatch and the constraints of the prior estimation (Cui et al., 2015). For this study, we focus on the seasonal-level evaluations, thereby we combine all data from each campaign (i.e each season) as one case, and derive the corresponding spatially- and temporally-resolved values of ε . We focus on the grid cells associated with the large values of influence functions for each campaign (details refer to Figure S3), and aggregate these grid cells in each sub-domain (i.e R1, R2, and R3 in Figure 3) according to the different ecoregions classified in the CarbonTracker system and obtain total 36, 36, 37 and 33 grid clusters for the four cases, respectively (more details in Figure S4). R is treated as the diagonal matrix in the study. We aggregated the time intervals from the native 3-hourly intervals to the daytime (14-01 UTC) and nighttime (02-13 UTC) scales of each day and used an e-folding temporal correlation scale (20days) to the same time period of day in the prior flux errors. We then calculate the weighted average of ε (without or within its sign) during each campaign, based on the temporal information constrained by $H^T H$ for each domain (i.e. R1, R2, and R3), to identify the seasonal error levels for the flux products.

250

3 Results and Discussion

251

252

253

254

255

256

As described in Section 2.5, we use both mole fraction-based and flux-based metrics to evaluate the four sets of NEE inversion products (e.g IS, LNLG, OG, and LNLGOGIS). First, the mole fraction-based RMSE analysis are shown in Figure 4. We found that the IS flux product has the best performance among the four products during the summer, fall, and spring, and has the second-best performance during the winter time. The performance of the LNLG flux product is second in most seasons and best in the

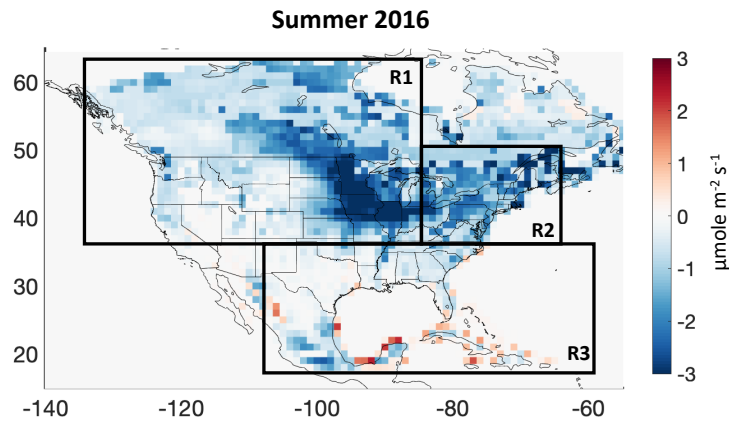


Figure 3. Three sub-domains are determined in the study: R1 denotes the Midwestern US and Western Canada areas; R2 denotes the Eastern US area; and R3 denotes the Southern US area. We only focus on the grid cells associated with the high values of the influence functions in the three domains. Details are described in Support Information. The background is the map of CO₂ NEE fluxes from the IS product, which are averaged values over July and August of 2016.

257 winter. The OG flux product has the worst performance across the winter, fall, and spring.
 258 The RMSE values integrated over four campaigns show that IS has the best aggregate
 259 performance at the annual level, followed by LNLG, OG, and LNLGOGIS. The multi-
 260 platform product (LNLGOGIS) performs similarly to the OG flux inversion.

261 We calculated the averaged absolute values of ε by campaign in Figure 5, based
 262 on equation (3). In general, the four flux products show similar spatial patterns during
 263 all four campaigns. The similar spatial patterns indicate that the spatial distributions
 264 of errors in the NEE of CO₂ estimates are not strongly dependent on the observational
 265 system used. All flux inversions show the largest errors in the Central and Eastern US
 266 during the summer time. There are larger errors in the Southern and Eastern US than
 267 other areas during the spring. The inversions in winter time show the smallest errors.
 268 Although the overall spatial patterns of errors are similar, some differences among the
 269 flux products can still be observed at the sub-regional scale. For example, LNLG and
 270 LNLGOGIS have similar overall performance with IS in Eastern and Southern US, but
 271 much worse than IS in Midwest and Western Canada.

272 We further calculate the seasonally averaged ε including the signs for the three sub-
 273 domains (Figure 6, and the corresponding spatial maps are shown in Figure S5) to iden-
 274 tify the seasonal errors for these regions in the flux products. Again, the spatial patterns
 275 of the seasonal errors in these CarbonTracker regional flux estimates are not strongly de-
 276 pendent on the observational data sources. During the summertime, we found that all
 277 inversions overestimate NEE of CO₂ in the Eastern US (so the magnitude of net pho-
 278 tosynthesis is underestimated), but significantly underestimate the flux (net photosyn-
 279 thesis is too large in magnitude) in the Midwest US and western Canada area from the
 280 LNLG and LNLGOGIS products. The LNLGOGIS product also underestimates NEE
 281 fluxes in the Southern US. The IS fluxes show the overall minimum errors across the three
 282 areas. The LNLG fluxes show similar errors with the IS fluxes in the Eastern and South-

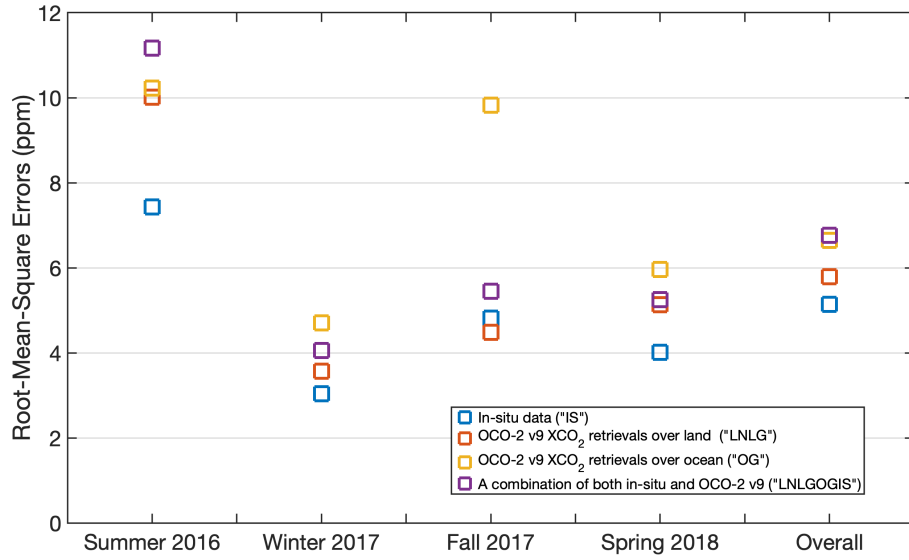


Figure 4. The Root-Mean-Square-Error (RMSE) between $y_{modelbio}$ and y_{ACTbio} from the four flux products are shown, for each ACT campaign (Summer 2016, Winter 2017, Fall 2017, and Spring 2018), and combined four campaigns (“overall”).

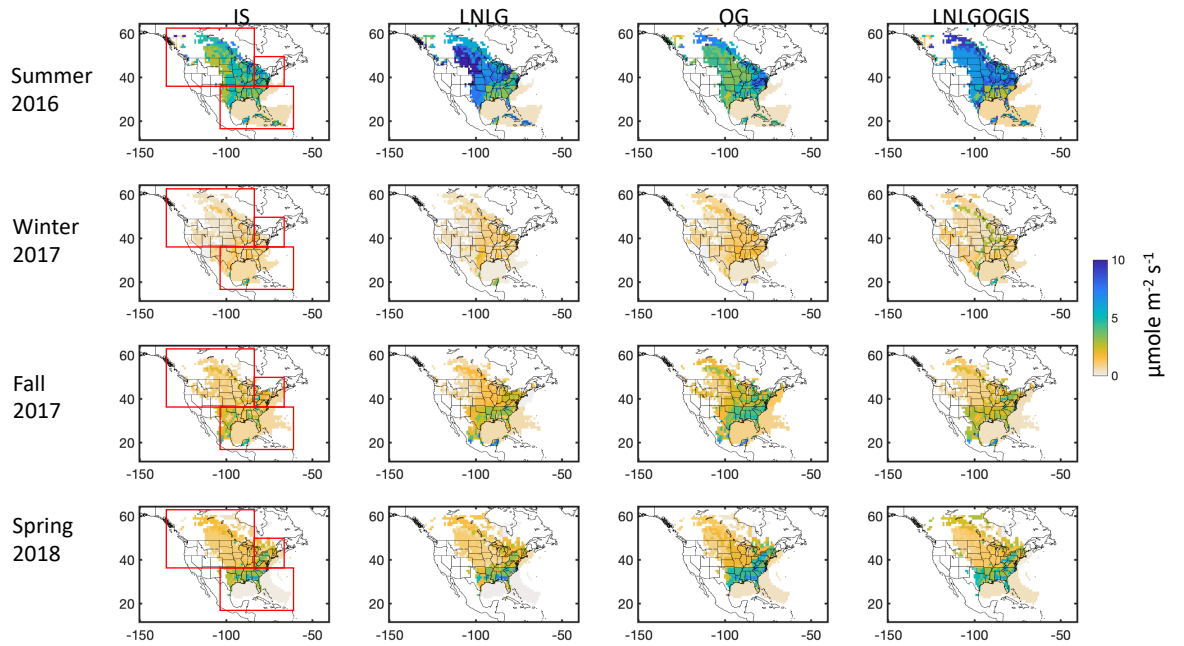


Figure 5. Spatial maps of the seasonally averaged ε values without the positive and negative signs corresponding to the four flux products during each ACT-America campaign, respectively.

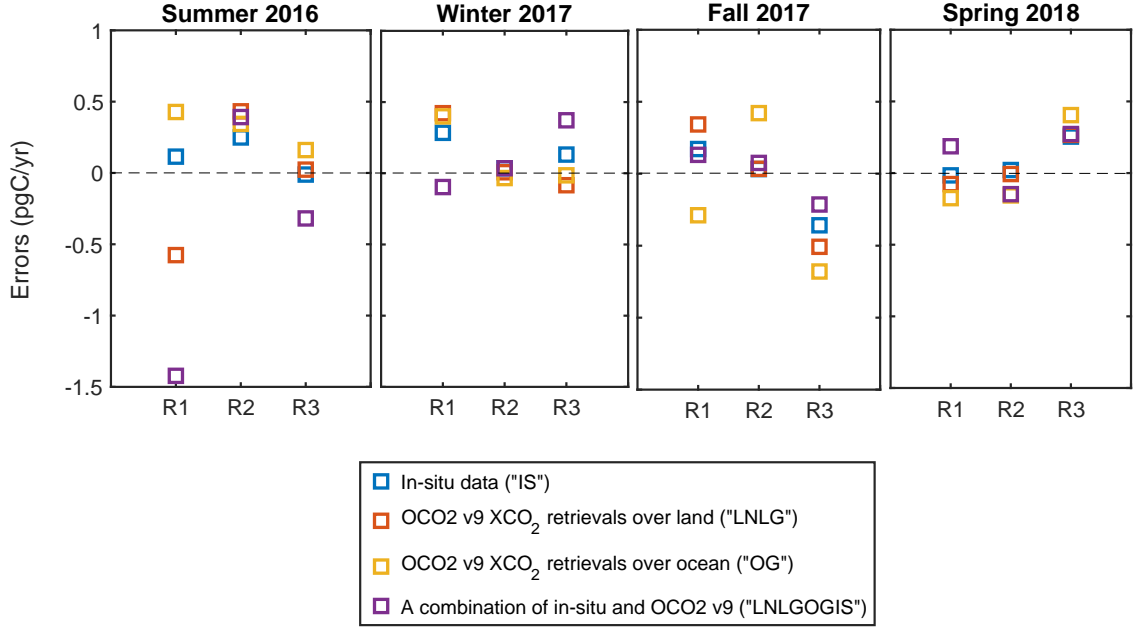


Figure 6. The integrated regional errors (ϵ values) refer to the daily flux estimation from the four flux products shown for each ACT-America campaign, respectively.

283 ern US, but larger errors than IS in the Midwest US and Western Canada area in sum-
 284 mer. Dormant season NEE is generally overestimated in the inversions. The LNLG fluxes
 285 show a larger overestimate of NEE in Midwest and Western Canada during the winter-
 286 time compared with IS, but show a smaller overestimate of NEE in the Eastern and South-
 287 ern US areas. During the fall, all inversions overestimate NEE of CO₂ in the Eastern US
 288 and underestimate NEE of CO₂ in the Southern US. The IS fluxes show fewer errors than
 289 the LNLG fluxes in the Midwest US and Western Canada and Southern US, but LNLG
 290 also shows a similar overestimate of NEE in the Eastern US during the fall. The OG fluxes
 291 show the largest errors across the three domains. All inversions overestimate NEE of CO₂
 292 in the Southern US during spring. The LNLG flux biases are similar in pattern and mag-
 293 nitude to the IS fluxes for the three domains.

294 Extrapolating these results across seasons suggests that the inversions generally am-
 295 plified the seasonal cycle of NEE in Midwest and Western Canada by underestimating
 296 summer NEE or overestimating dormant season NEE, especially for the LNLG products.
 297 When we consider ϵ results across the four campaigns we found that the annual NEE
 298 of CO₂ fluxes have the positive errors in in Midwest and Western Canada and Eastern
 299 US from the IS and LNLG fluxes, but the LNLG fluxes show negative errors in the South-
 300 ern US. The IS fluxes have the best seasonal performance and LNLG has the best annual
 301 performance across the three areas (i.e the Central and Eastern temperate North
 302 America).

303 The seasonally averaged ϵ by daytime and nighttime for each case are calculated
 304 as well (Figure S6 and S7), respectively. The spatial patterns of the errors during the
 305 daytime and nighttime largely match those found for the daily NEE error estimates in

306 Figure 6. During the summertime, opposing patterns of ε (negative values during the
 307 daytime, and positive values during the nighttime) in Midwest and Western Canada sug-
 308 gest that both nighttime respiration and net daytime photosynthesis are overestimated
 309 in the area. Both positive biases during daytime and nighttime in the Eastern US sug-
 310 gest overestimated biogenic respiration in this region. During the wintertime, positive
 311 biases seen in day and night from IS and LNLG in Midwest and Western Canada indi-
 312 cate that respiration is overestimated in the region. The magnitudes of errors in day and
 313 night from all flux products are small in the Eastern US. Opposing patterns of ε (neg-
 314 ative values during the daytime, and positive values during the nighttime) are seen in
 315 the Southern US. Consequently, the overall daily errors in these areas are small in Fig-
 316 ure 6. In the fall, opposing patterns of ε (negative values during the daytime, and pos-
 317 itive values during the nighttime) are seen again in the Southern US. In the spring, op-
 318 posing patterns of ε (negative values during the daytime, and positive values during the
 319 nighttime) in the three domains suggest that both nighttime respiration and net day-
 320 time photosynthesis are overestimated in these areas.

321 4 Conclusions

322 We implement a framework to evaluate the NEE of CO₂ flux estimations across
 323 the Central and Eastern United States and some of Western Canada. We use this ap-
 324 proach on the posterior fluxes from the CarbonTracker global flux inversion system, which,
 325 for the OCO2 v9 MIP, was run with four different atmospheric CO₂ data sources.

326 This study suggests that, in terms of regional variability in NEE of CO₂, the in situ
 327 (IS) inversion and the inversion using the land-nadir, land-glint (LNLG) observations
 328 from OCO-2 v9 are likely to be the most reliable products of the CarbonTracker system,
 329 superior to inversions based on the OCO-2 v9 ocean-glint (OG) or all data platforms (LNL-
 330 GOGIS) data sets. We found, using a error diagnosis metric, that IS generally outper-
 331 forms the inversions based on OCO-2 v9 observations, but the differences between the
 332 IS inversion and the LNLG inversion are relatively small. The OG and LNLGOGIS in-
 333 versions are clearly inferior to the IS and LNLG inversions with respect to this error met-
 334 ric analysis, and warrant further investigations. This strong performance of the LNLG
 335 inversion as compared to the IS inversion is encouraging when considering inverse flux
 336 estimates in regions of the world where the in situ observing network is sparse.

337 The spatially resolved errors for the regional fluxes in CarbonTracker are not strongly
 338 dependent on the observational data source. Our results suggest that CarbonTracker over-
 339 estimates seasonal NEE for the Central and Eastern US, and that, as a result, the an-
 340 nual NEE from CarbonTracker may underestimate continental uptake of CO₂ (annual
 341 mean NEE too positive). Summer NEE is positively biased in the Eastern US and neg-
 342 atively biased in Midwest and Western Canada, yielding relatively little total seasonal
 343 bias across the continent in summer. In the dormant seasons, the CarbonTracker inver-
 344 sions appear generally to overestimate NEE. It is possible that the FLEXPART-WRF
 345 transport model used in our evaluation system may be biased. Conclusive assessment
 346 of the magnitude of the errors in seasonal NEE from CarbonTracker will depend on a
 347 more rigorous assessment of the transport models, which is currently being conducted.
 348 Nevertheless, we demonstrate that this continental-scale, multi-season airborne dataset
 349 provides sufficient data to distinguish among inverse flux estimates and posterior iden-
 350 tify flux biases, resulting in better understanding of the true NEE from North America.

351 We propose to extend this evaluation framework to other flux products from both
 352 top-down or bottom-up methods, such as other members of the OCO-2 v9 MIP and any
 353 available continental-scale biogenic CO₂ flux estimates. We hypothesize that these stud-
 354 ies will yield insights that are applicable across the globe, especially in midlatitude ecosys-
 355 tems.

Acknowledgments

The Atmospheric Carbon and Transport (ACT) - America project is a NASA Earth Venture Suborbital 2 project funded by NASA's Earth Science Division (Grant NNX15AG76G to Penn State). We also would like to acknowledge the support for the OCO-2 v9 flux model inter-comparison project provided through NASA grant #80 NSSC 18K0909. We gratefully thank Joshua P. DiGangi, Bianca Baier who led the measurements of CO₂ in the ACT-America campaign, Yaxing Wei and Gao Chen who led data archival efforts, and Thomas Lauvaux who participated the design of the WRF-Chem modeling configuration. The authors declare, to their knowledge, no conflicts of interest with the submission of this manuscript. FLEXPART-WRF model can be found online (<https://www.flexpart.eu/wiki/FpLimitedareaWrf>). All ACT-America in situ data used in the manuscript can be found online (https://daac.ornl.gov/cgi-bin/dsvviewer.pl?ds_id=1593). The WRF-Chem simulations used in the manuscript can be found online (<https://doi.org/10.26208/49kd-b637>), and FLEXPART-WRF simulations can be found online (ftp://evs2ftp.ornl.gov/Inversion_Models/Influence_Function/).

References

- Andrews, A. E., Kofler, J. D., Trudeau, M. E., Williams, J. C., Neff, D. H., Masarie, K. A., ... Tans, P. P. (2014). CO₂, CO, and CH₄ measurements from tall towers in the NOAA Earth System Research Laboratory's global greenhouse gas reference network: instrumentation, uncertainty analysis, and recommendations for future high-accuracy greenhouse gas monitoring efforts. *Atmospheric Measurement Techniques*, 7(2), 647–687.
- Baier, B. C., Sweeney, C., Choi, Y., Davis, K. J., DiGangi, J. P., Feng, S., ... Weibring, P. (2020). Multispecies assessment of factors influencing regional and enhancements during the winter 2017 act-america campaign. *Journal of Geophysical Research: Atmospheres*, 125(2), e2019JD031339.
- Brioude, J., Arnold, D., Stohl, A., Cassiani, M., Morton, D., Seibert, P., ... Wotawa, G. (2013). The Lagrangian particle dispersion model flexpart-wrf version 3.1. *Geoscientific Model Development*, 6(6), 1889–1904.
- Chevallier, F., Remaud, M., O'Dell, C. W., Baker, D., Peylin, P., & Cozic, A. (2019). Objective evaluation of surface- and satellite-driven carbon dioxide atmospheric inversions. *Atmospheric Chemistry and Physics*, 19(22), 14233–14251.
- Ciais, P., Dolman, A. J., Bombelli, A., Duren, R., Peregon, A., Rayner, P. J., ... Zehner, C. (2014). Current systematic carbon-cycle observations and the need for implementing a policy-relevant carbon observing system. *Biogeosciences*, 11(13), 3547–3602.
- Crowell, S., Baker, D., Schuh, A., Basu, S., Jacobson, A. R., Chevallier, F., ... Jones, D. B. A. (2019). The 2015–2016 carbon cycle as seen from OCO-2 and the global in situ network. *Atmospheric Chemistry and Physics*, 19(15), 9797–9831.
- Cui, Y. Y., Brioude, J., Angevine, W. M., Peischl, J., McKeen, S. A., Kim, S.-W., ... Trainer, M. (2017). Top-down estimate of methane emissions in California using a mesoscale inverse modeling technique: The San Joaquin Valley. *Journal of Geophysical Research: Atmospheres*, 122(6), 3686–3699.
- Cui, Y. Y., Brioude, J., McKeen, S. A., Angevine, W. M., Kim, S.-W., Frost, G. J., ... Trainer, M. (2015). Top-down estimate of methane emissions in California using a mesoscale inverse modeling technique: The South Coast Air Basin. *Journal of Geophysical Research: Atmospheres*, 120(13), 6698–6711.
- Cui, Y. Y., Henze, D. K., Brioude, J., Angevine, W. M., Liu, Z., Bousserrez, N., ... Trainer, M. (2019). Inversion estimates of lognormally distributed methane emission rates from the Haynesville-Bossier oil and gas production region using airborne measurements. *Journal of Geophysical Research: Atmospheres*,

- 409 124(6), 3520-3531.
- 410 Davis, K., Obland, M., Lin, B., Lauvaux, T., O'Dell, C., Meadows, B., ... Pauly,
411 R. (2018). Act-america: L3 merged in situ atmospheric trace gases and
412 flask data, eastern usa. *ORNL DAACm, Oak Ridge, Tennessee, USA.*,
413 <https://doi.org/10.3334/ORNLDAAC/1593>.
- 414 Eldering, A., O'Dell, C. W., Wennberg, P. O., Crisp, D., Gunson, M. R., Viatte, C.,
415 ... Yoshimizu, J. (2017). The orbiting carbon observatory-2: first 18 months
416 of science data products. *Atmospheric Measurement Techniques*, 10(2), 549–
417 563.
- 418 Eldering, A., Wennberg, P. O., Crisp, D., Schimel, D. S., Gunson, M. R., Chatter-
419 jee, A., ... Weir, B. (2017). The orbiting carbon observatory-2 early science
420 investigations of regional carbon dioxide fluxes. *Science*, 358(6360).
- 421 Feng, S., Lauvaux, T., Davis, K. J., Keller, K., Zhou, Y., Williams, C., ... Baker, I.
422 (2019a). Seasonal characteristics of model uncertainties from biogenic fluxes,
423 transport, and large-scale boundary inflow in atmospheric co2 simulations
424 over north america. *Journal of Geophysical Research: Atmospheres*, 124(24),
425 14325-14346.
- 426 Feng, S., Lauvaux, T., Keller, K., Davis, K. J., Rayner, P., Oda, T., & Gurney,
427 K. R. (2019b). A road map for improving the treatment of uncertainties in
428 high-resolution regional carbon flux inverse estimates. *Geophysical Research*
429 *Letters*, 46(22), 13461-13469.
- 430 Hayes, D. J., Turner, D. P., Stinson, G., McGuire, A. D., Wei, Y., West, T. O., ...
431 Cook, R. B. (2012). Reconciling estimates of the contemporary north american
432 carbon balance among terrestrial biosphere models, atmospheric inversions,
433 and a new approach for estimating net ecosystem exchange from inventory-
434 based data. *Global Change Biology*, 18(4), 1282-1299.
- 435 Haynes, K. D., Baker, I. T., Denning, A. S., Stöckli, R., Schaefer, K., Lokupitiya,
436 E. Y., & Haynes, J. M. (2019). Representing grasslands using dynamic prog-
437 nostic phenology based on biological growth stages: 1. implementation in the
438 simple biosphere model (sib4). *Journal of Advances in Modeling Earth Sys-*
439 *tems*, 11(12), 4423-4439.
- 440 Hersbach, H., Bell, B., Berrisford, P., Hirahara, S., Horányi, A., Muñoz-Sabater, J.,
441 ... Thépaut, J.-N. (2020). The era5 global reanalysis. *Quarterly Journal of*
442 *the Royal Meteorological Society*, 146(730), 1999-2049.
- 443 Hu, L., Andrews, A. E., Thoning, K. W., Sweeney, C., Miller, J. B., Michalak,
444 A. M., ... van der Velde, I. R. (2019). Enhanced north american carbon
445 uptake associated with el niño. *Science Advances*, 5(6).
- 446 Jacobson, A. R., Schuldt, K. N., Miller, J. B., Oda, T., Tans, P., Andrews, A.,
447 ... Zimnoch, M. (2020). Carbontracker ct2019. *Model published by*
448 *NOAA Earth System Research Laboratory, Global Monitoring Division, 2020.*
449 <https://doi.org/10.25925/39m3-6069>.
- 450 Keller, K., McInerney, D., & Bradford, D. F. (2008). Carbon dioxide sequestration:
451 how much and when? climatic change. *Climatic Change*, 88(8), 267.
- 452 Liu, J., Baskaran, L., Bowman, K., Schimel, D., Bloom, A. A., Parazoo, N. C., ...
453 Wofsy, S. (2020). Carbon monitoring system flux net biosphere exchange 2020
454 (cms-flux nbe 2020). *Earth System Science Data Discussions*, 2020, 1–53.
- 455 Liu, J., Bowman, K. W., Schimel, D. S., Parazoo, N. C., Jiang, Z., Lee, M., ... El-
456 dering, A. (2017). Contrasting carbon cycle responses of the tropical continents
457 to the 2015–2016 el niño. *Science*, 358(6360). doi: 10.1126/science.aam5690
- 458 Masson-Delmotte, V., Zhai, P., Pörtner, H. O., Roberts, D., Skea, J., Shukla, P.,
459 ... Waterfield, T. (2018). Ipcc, 2018: Global warming of 1.5°C. an ipcc special
460 report on the impacts of global warming of 1.5°C above pre-industrial
461 levels and related global greenhouse gas emission pathways, in the context of
462 strengthening the global response to the threat of climate change, sustainable
463 development, and efforts to eradicate poverty. *In press*.

- 464 Miles, N. L., Richardson, S. J., Davis, K. J., Lauvaux, T., Andrews, A. E., West,
465 T. O., ... Crosson, E. R. (2012). Large amplitude spatial and temporal gra-
466 dients in atmospheric boundary layer co2mole fractions detected with a tower-
467 based network in the u.s. upper midwest. *Journal of Geophysical Research:*
468 *Biogeosciences*, 117(G1).
- 469 Miller, S. M., & Michalak, A. M. (2020). The impact of improved satellite re-
470 trievals on estimates of biospheric carbon balance. *Atmospheric Chemistry and*
471 *Physics*, 20(1), 323–331.
- 472 Ogle, S. M., Davis, K., Lauvaux, T., Schuh, A., Cooley, D., West, T. O., ... Den-
473 ning, A. (2015). An approach for verifying biogenic greenhouse gas emissions
474 inventories with atmospheric CO2 concentration data. *Environmental Research*
475 *Letters*, 10(3), 034012.
- 476 Pan, Y., Birdsey, R. A., Fang, J., Houghton, R., Kauppi, P. E., Kurz, W. A., ...
477 Hayes, D. (2011). A large and persistent carbon sink in the world's forests.
478 *Science*, 333(6045), 988–993.
- 479 Rayner, P. (2020). Data assimilation using an ensemble of models: a hierarchical ap-
480 proach. *Atmospheric Chemistry and Physics*, 20(6), 3725–3737.
- 481 Thompson, R. L., Broquet, G., Gerbig, C., Koch, T., Lang, M., Monteil, G., ...
482 Rödenbeck, C. (2020). Changes in net ecosystem exchange over europe during
483 the 2018 drought based on atmospheric observations. *Philosophical Transac-*
484 *tions of the Royal Society B: Biological Sciences*, 375(1810), 20190512.
- 485 Tian, H., Lu, C., Ciais, P., Michalak, A., Canadell, J., Saikawa, E., ... Wofsy, S.
486 (2016). The terrestrial biosphere as a net source of greenhouse gases to the
487 atmosphere. *Nature*, 531, 225–228.
- 488 Wei, Y., Shrestha, R., Pal, S., Gerken, T., McNelis, J., Singh, D., ... Davis, K. (in
489 prep for this issue). The atmospheric carbon and transport (act) – america
490 datasets: Description, management, and delivery. *Earth and Space Science*.